Chapter 13
Connecting Rod

Prakash R. Wani

Abstract The connecting rod converts the reciprocating motion of piston into the rotating motion of the crankshaft. Generally, it can be seen in three parts, i.e., small end, shank and big end. The connecting rod motion is complex as the small end is reciprocating along cylinder axis and big end is rotating along with the crankpin. The Loads on a connecting rod are categorized as three types namely, Firing load, Inertia load and other loads. The analysis of loads on Connecting Rod by classical method must be carried out for sizing and shaping before going for detailed analysis using the finite element method for both static and dynamic loads. The examples for the classical method are available in the appendix. The analysis for the four load cases namely, Bolt Preload and Bearing and Bush Interference, Gas Pressure Loading, Inertia Loading and Combined Loading is presented. Enhancing the yield strength and fatigue strength is achieved by choice of Materials and heat treatment. Some practical aspects during design like Weight grouping of connecting rods, Push-out force test and Testing of the connecting rod are given. The fracture splitting method for connecting rods is becoming popular as an exercise in cost reduction. The manufacturing process of connecting rod is described in brief. At the end of the chapter various failure modes are described which are borne in mind while designing the connecting rod.

13.1 Introduction

The connecting rod is an important element of engine that joins the piston and the crankshaft. It is used to achieve the rotating motion of the crankshaft from the reciprocating motion of piston. Normally it consists of small end that reciprocates with piston, big end which is attached at crankpin of a crankshaft and the shank portion that joins small and big ends.

P. R. Wani (✉)
Government College of Engineering, Karad, India
e-mail: pwani51@gmail.com

P. A. Lakshminarayanan and A. K. Agarwal (eds.), *Design and Development of Heavy Duty Diesel Engines*, Energy, Environment, and Sustainability,
https://doi.org/10.1007/978-981-15-0970-4_13

Depending on the fixation of piston pin the construction of small end can vary. In floating piston arrangement, there is a clearance between the piston and piston pin. The piston pin is fixed at the small end. This arrangement results in compact design of the piston pin. In case of floating piston pin, the connecting rod at small end is provided with the bush. The piston pin is axially stopped by two circlips with the help of grooves provided in the piston. For highly loaded engines the use of floating pins is popular. The cross section of the shank of the connecting rod is normally of I-shaped to resist buckling.

The big end of the connecting rod is normally split so that the connecting rod and the cap are formed to facilitate the assembly and dismantling the connecting rod from the crankshaft. The split can be avoided if the construction of the crankshaft is of built-type, i.e., the crankshaft is now split having parts like crankpin and webs with bore to suit the crankpin assembly. The former arrangement is popularly used in case of assembly and maintenance point of view. The split of the connecting rod may be perpendicular to the connecting rod axis or inclined. The inclined split connecting rods permit increased big end bore diameter and still assembly is possible through the cylinder bore. In split connecting rod and cap, it is important that these two parts are located properly during operation of the engine. If the alignment is not maintained properly the bearing life and performance is hampered. Also, fretting failure may take place at the joint of the connecting rod and cap.

To locate the cap with respect to the connecting rod the arrangements like serrations, tongue and groove type of construction are used along with dowel pin or fitted bolts. It is important that the mating faces of the connecting rod and the cap are in contact properly. The tendency of fretting is increased if the area in contact is reduced. Nowadays, some of the connecting rods are split at big end by fracture technology. The notching is done at the inner diameter by laser and the oversize mandrel with taper is pressed into the semi-finished big end bore. This results into a fracture split connecting rod, where almost 100% area of the contact is assured. However, in such cases the material of the connecting rod should be chosen with care. With this process, the manufacturing cost is appreciably reduced. However, the initial investment in machinery is high. To locate the bearing shell in rod and cap a notch or dowel is provided. It should be ensured that the bearing is not fouling with the rotating part of crankpin or fillet.

In case of highly loaded engines the pistons require cooling, which is provided by the oil. The drilling through the connecting rod big end or shank should leave sufficient wall thickness around this drilled hole. Sometimes, pressurized oil is provided to the small end bearing through the drilling made inside the connecting rod.

13.2 Loads on a Connecting Rod

Firing load

During combustion, the piston is subjected to the firing pressure. The forces acting on the piston are transferred to the piston pin and then to the connecting rod. The maximum load on the connecting rod due to firing pressure,

$$maximum\ load\ on\ piston = \frac{\pi}{4} D^2 pfp$$

where

pfp = peak firing pressure and
D = piston diameter

Inertia load

Inertia force is induced due to the motion of the piston along the cylinder axis. It acts along the cylinder axis. The magnitude of inertia force is the product of the reciprocating mass and acceleration. The mass of the piston assembly and some fraction of the connecting rod which can be assumed as the reciprocating mass needs to be considered for this calculation. The portion of this reciprocating mass and the acceleration of the reciprocating mass can be evaluated as discussed in Appendix 1 Distribution of connecting rod mass at small end and big end can be shown as follows.

$$W_{assly} = W_{recip} + W_{rot}$$

$$W_{assly} = W_{recip}\left(\frac{L_1 + L_2}{L_2}\right)$$

Or

$$W_{recip} = W_{assly}\left(\frac{L_2}{L_1 + L_2}\right)$$

The displacement x of piston assembly from the TDC at the time when the crank angle is θ, can be shown to be

$$\therefore x = (L + R) - (L\cos\varphi + R\cos\theta)$$

Or

$$\begin{gathered}\frac{x}{R} = 1 + \frac{\lambda}{4} - \cos\theta - \frac{\lambda}{4}\cos 2\theta \\ velocity, v = \dot{x} = \omega R\left(\sin\theta + \frac{\lambda}{2}\cos 2\theta\right) \\ acceleration, a = \dot{v} = \ddot{x} = \frac{dv}{d\theta}\frac{d\theta}{dt} = \frac{dv}{d\theta}\omega \\ = R\omega^2\left(\cos\theta + \frac{\cos 2\theta}{n}\right)\end{gathered}$$

where

$$n = \frac{1}{\lambda}$$

$$\therefore Inertiaload = m_{recip} \times acceleration = m_{recip}R\omega^2\left(\cos\theta + \frac{\cos 2\theta}{n}\right)$$

This force is varying with respect to crank angle θ. The first part involving cosine θ term is called the primary inertia force and the second part involving cosine 2θ is called the secondary inertia force. The frequency of the secondary force is twice that of the primary inertia force.

$$maximum\,inertia\,force = m_{recip}R\omega^2\left(1 + \frac{1}{n}\right)$$

where

$$\theta = 0, \pi, 2\pi, \ldots$$

It is to be noted that the maximum firing load and the maximum inertia load are not acting at the same instance. Generally, at the start of suction stroke for a four-stroke cycle engine, the inertia force may be predominant while at the start of the power stroke, firing load may be predominant. Thus, in a working cycle the load is fluctuating. As the inertia load is opposing the firing load at firing TDC position, the resultant load is reduced to that extent.

Other loads

The dimensions of cross section of the shank are based on the buckling load. The permissible buckling load as per Rankine-Gordon formula for a beam under compression is

$$F_{xx} = \frac{f_c A}{1 + a\left(\frac{l}{R_{xx}}\right)^2}$$

where

F_{xx} = *critical load with respect to xx axis of the cross section*

F_c = *allowable compressive stress*
A = *minimum cross section area of the shank*
$\boldsymbol{a}$ = *constant depending on material*

$\left(\frac{l}{R_{xx}}\right)$ = *slenderness ratio*
L = *length of the connecting rod from small end to big end*

R_{xx} *is the radius of gyration of cross section about xx axis*

The whipping stress acting on the cross section is calculated as follows. The average maximum whipping force acting due to the weight of the connecting rod is

$$F_i = \frac{\rho A l}{2g} R\omega^2$$

where

ρ = *weight density of connecting rod material*
A = *cross section area*
R = *crank throw or crank radius*
l = *length of connecting rod*
Fi = *Force on connecting rod due to rotation*

Maximum bending moment,

$$M_{max} = \frac{2F_i l}{g\sqrt{3}}$$

Maximum whipping stress,

$$\sigma_b = \frac{M_{max}}{Z} = \frac{M_{max}}{\left(\frac{I}{y}\right)}$$

where

I = *area inertia of the cross section*
y = *distance of outermost fibre from the neutral centre of I section*

The dimensions of small end bearing side diameter and length can be estimated by application of bearing stress criterion, i.e.

$$\text{Allow able bearing stress} = \frac{F_{max}\text{on small end}}{\text{projected bearing area}} = \frac{F_{max}}{\text{diameter of small end} \times \text{length of bearing at small end}}$$

A similar criterion can be applied for the big end. As the small end bush or big end bearing should be fitted in such a way to avoid the rotation relative to the housing, the radial and hoop stresses may be calculated by applying the thick and thin composite cylinder theory.

13.3 Load Analysis of Connecting Rod by Classical Method

In general, for the connecting rod analysis the I-section calculations are performed to confirm that sufficient margin is available against the critical buckling load. The section with minimum cross section area is chosen for such calculations. The increase in stresses due to stress concentration factor at the junctions is either taken approximately or factor of safety requirements are increased accordingly. As a guideline I section dimensions with proportion of 4T-5T-T are usually assumed. The details of reasoning are explained in the Appendix 2.

The small end and big end calculations are done with some approximations by applying the curved beam theory. Please refer Appendix 3 for details (Bremi 1971). The interference fit between the small end bush and the connecting rod is treated as the composite cylinder so that radial and hoop stresses can be calculated. Similar treatment can be given at big end. At the big end, if the connecting rod is split and bolting is used, it is necessary to consider additional load due to bolt clamping.

The calculation of big end bolt can be performed based on the standard VDI 2230 (VDI 2230). The sample calculation for a typical case is shown in Appendix 4.

Whipping stresses are combined with the stresses due to firing loads and inertia loads. The maximum compressive stress and maximum tensile stress are taken for approximate calculation of fatigue stress. It is then compared with the endurance stress of the material chosen for the connecting rod.

Additional aspects like manufacturing variations should be given due consideration so that variation of dimensions and mechanical properties are covered while finalising the design.

13.4 Load Analysis of Connecting Rod by Finite Element Method

Analysis Details

It is observed that peak firing pressure in diesel engines occurs after the TDC (top dead centre) position. However, for initial simulation it can assumed as occurring at TDC. Maximum inertia load will act at TDC position.

An axis-symmetric model of Connecting Rod Subassembly is modelled. The model is meshed, assembled and material properties are applied (Pravardhan 2004). Figure 13.1 shows some critical locations for stress calculations in a connecting rod.

Load Cases:

Case 1: **Bolt Preload and Bearing and Bush Interference**

In case of the split connecting rods the cap and rod are fastened together with nut and bolt type of arrangement. The tightening of the bolt with the nut or inside the tapping of the connecting rod is required to hold these parts including the big end bearing. This assembly induces the compressive loads in the connecting rod and cap. Due to tightening the bolt gets stretched and is subjected to the tensile load. The bearings at the small end and at the big end are subjected to the loads caused by the interference fit. The stresses due to such assembly conditions are in fact present in the parts even before the engine is in operation. This case is simulated and treated as the preload on the assembly.

Case 2: **Gas Pressure Loading**

The contact condition of the piston pin and the bush is considered as clearance fit. Similarly, at the crank pin bearing, clearance is considered. Crank pin is modelled as rigid surface and constrained in all 6 degrees of freedom. The bolt is included in the model, but not preloaded. One fourth of this maximum gas force is applied on

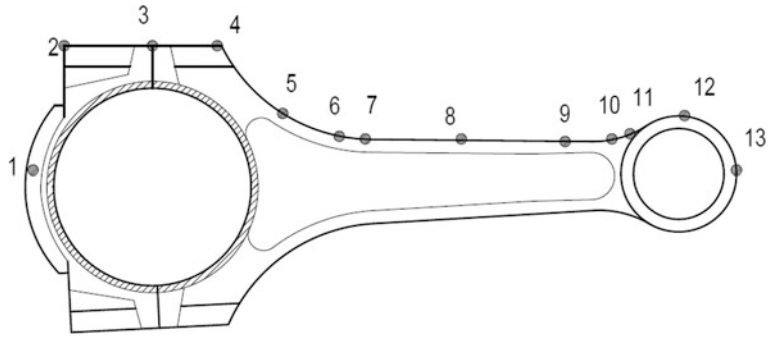

Fig. 13.1 A typical stress distribution at some locations of a connecting rod

the piston pin. For application of this force reference point is created and then it is coupled to the piston pin upper surface.

Case 3: **Inertia Loading**

The inertia force is calculated at maximum over-speed condition. The bolt is included in the model, but not preloaded. One fourth of this maximum inertia force is applied on the piston pin considering symmetric model. For application of this force a reference point is created and then it is coupled to the piston pin lower surface. In this case the possibility of split line separation is also evaluated during inertia loading of the connecting rod.

Case 4: **Combined Loading**

In this case the two combined loadings are simulated.

$$\begin{aligned} Combined\ load1 = {} & bolt\ load + bearing\ bust\ interference\ load \\ & + gas\ pressure \end{aligned}$$

and

$$\begin{aligned} Combined\ load2 = {} & bolt\ load + bearing\ bust\ interference\ load \\ & + inertia\ load \end{aligned}$$

Most of points on shank subjected to more compressive stresses and the points at outer side of big end and small end are subjected to more tensile stresses. The points at the junctions of small end to I section and at big end to I section are subjected to multi axial state of stress. The equivalent stress amplitude can be calculated based on Von Mises criterion, as follows:

$$S_{qa} = \sqrt{\frac{\left(S_{ax} - S_{ay}\right)^2 + \left(S_{ay} - S_{az}\right)^2 + \left(S_{az} - S_{ax}\right)^2 + 6\left(t_{axy}^2 + t_{ayz}^2 + t_{azx}^2\right)^2}{2}}$$

The equivalent mean stress is calculated as follows:

$$S_{qm} = S_{mx} + S_{my} + S_{mz}$$

It had been observed that mean shear stress had no effect on cyclic bending or cyclic torsion fatigue limits. After obtaining the equivalent mean stress and stress amplitude, the equivalent stress amplitude at R = -1 (corresponds to S_{Nf}) was obtained by using the commonly used modified Goodman equation:

$$\frac{S_{qa}}{S_{Nf}} + \frac{S_{qm}}{S_u} = 1$$

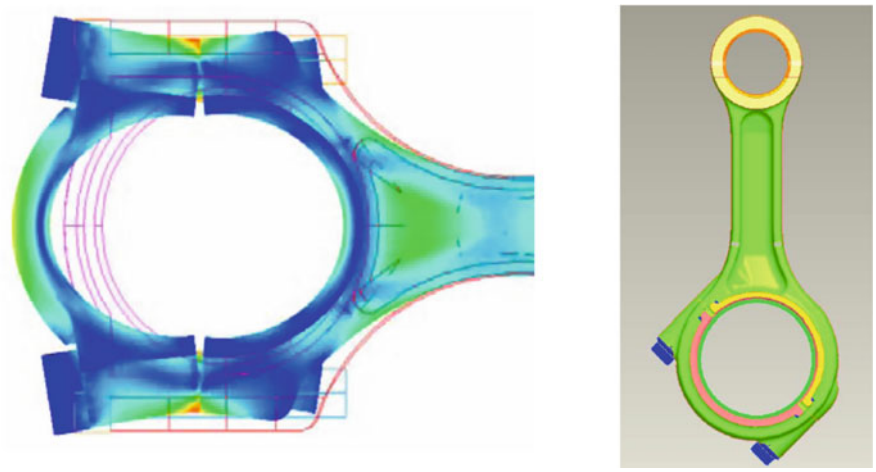

Fig. 13.2 A model and typical stress distribution at some locations of a connecting rod

The Fig. 13.2 shows the model of rod and the stresses at big end.

Initial rough calculations can be performed on 2D FE models as it can be completed relatively quickly. Once the trend is known 3D FE models can be used for more detailed analysis.

Various factors can be considered for optimization of the connecting rod. Generally, cost optimization is main objective to deal with the competition in the market. However, in some applications like defence, the packaging dimensions may have more importance. The limited life, high cost material may be allowed in such cases to obtain the compact equipment. To be on the conservative side the maximum tensile load is taken as the load at maximum speed and assumed to be occurring at TDC. Also, for the compressive load calculations peak firing pressure is considered.

The manufacturing constraints need to be given a proper thought at the design stage.

Depending on the material selected and the mechanical properties sufficient factor of safety should be assured against the buckling load. Fatigue strength is the most significant factor (i.e., design driving factor) in the design and optimization of the connecting rod. To design for fatigue, modified Goodman equation may be used. The fatigue stress amplitude and the maximum stress value should be less than the allowable values.

Additional constraints imposed during the optimization process may be maintaining the forge ability as well as interchange ability of the connecting rod with the existing one. Cost may be reduced by changing the material to crackable forged steel in place of regular steel forging.

13.5 Materials and Heat Treatment

For the connecting rods of engines with low brake mean effective pressure generally the low-cost material is preferred. Hardenable medium carbon materials like CK 45, En9, and En8D are used in normalised, quenched and tempered condition. For high BMEP engines generally materials like En16, 42CrMo4 are used in NQT condition. The failure of the connecting rod may result into breakage of surrounding parts. In such cases the elongation of the steel material reduces the damage to some extent. Spheroidal Graphite iron material of grade 600 or 700 is sometimes used for low duty connecting rods. However, to remove the bend or twist of such rods is very difficult during the manufacturing process.

For fracture split connecting rods the crackable steel material C-70 is used. It is expected in this case that the brittle crack is formed at the big end of the connecting rod at the time of splitting process.

13.6 Some Practical Aspects During Design

The connecting rod experiences the combination of different loads. The varying cyclic load acting on the rod makes it critical from durability aspect. Being one of the central parts of the engine, deep thought is required during design stage itself. If there is a change in dimensions of the connecting rod, the other parts in the vicinity may require the alterations those may be difficult to accommodate. The changes in connecting rod processing are also costly and time consuming. For these reasons the study of latest production technologies, finite element modelling and simulations, optimization techniques are usually applied. Application of new materials is also the subject of research for making of the connecting rods.

If the connecting rod is split perpendicular to the connecting rod axis, the nut and the bolt arrangement may be used to clamp the cap with the rod. In such cases the bolt head is special so that it locks the bolt rotation while tightening the nut. When the connecting rod split is inclined the bolt is used with tapping on the connecting rod. In such a case no nut is required. Normally, one of the tapping is blind and hence the minimum wall thickness around the tapped hole must be critically ensured. In vee engines, if the connecting rods are placed side by side, the size of the inside chamfer of the big end bore can be reduced the two connecting-rod mating side. This can be possible as there is no question of crank pin fillet riding on the bearing. If compact size of engine is desired in vee engines, a pair of articulated master and slave rod is used. In such a case it is like a radial engine with a hole at big end on the master rod that accommodates the big end of the slave rod. For such engines, the stroke of the two piston rod assemblies is slightly different.

It must be ensured from the layouts that Connecting rod is not interfering with other parts like crankcase, cylinder liner, piston, piston cooling nozzles, balance weights etc.

Dimensional and form tolerances on big end bore diameter, small end bore, centre to centre distance between the big end and small end, bend and twist should be kept as minimum as possible. The bolt-hole axis should be maintained square to the mating faces.

In case of the split connecting rods, the tightening of the bolts is an important aspect. These bolts are used for holding the rod, cap and big end bearings together. The torque on the bolt induces the preload on the bolt and other mating parts. The systematic calculations for the bolted joint can be performed by referring to VDI 2230 standard (VDI 2230). If the split of the connecting rod is inclined, the bolts must also resist the side force. The magnitude of the side force Q can be evaluated based on equations in Appendix 3. Usually for this purpose the connecting rods are serrated at the parting faces. Some connecting rods may have tongue and groove type of arrangement. With serrations or tongue-groove combination it is possible to restrict the motion of cap relative to connecting rod in the plane of their parting surfaces.

13.6.1 Weight Grouping of Connecting Rods

As the inertia force due to connecting rod mass is varying in magnitude during engine running, it creates varying force on the foundation for a single cylinder engine. To have the consistent behaviour of the engine, the weight of the connecting rod and the piston assembly should be in a closed interval and not with wide spread. For multiple cylinder engines, it becomes necessary to control the weights of the connecting rods in the same engine to maintain the inertia force magnitude at equal level. In case of high-speed engines, the control on distribution of weight is important. Close tolerance on weight distribution can keep vibrations are under control. The weight of the connecting rod can be adjusted by removal of material that is provided additionally on the big end and or small end side. This removal should not impair the strength against the operational loading on the connecting rod.

13.6.2 Push-Out Force Test

The interference force between the bush and the connecting rod resists the rotation of small end bush. This resistance is proportional to the push out force. The push out force is the force required to push the bush from its assembled position in the connecting rod. Generally, a suitable fixture is made to find this force and it can be estimated by a load cell or on a universal testing machine. The push out force is dependent on the interference between the mating parts. It also depends on the modulus of elasticity of the assembled components, surface finish of the components and the assembly process e.g., use of hand press or liquid nitrogen etc. (Wani et al. 2005).

13.6.3 Testing of the Connecting Rod

The design calculations are generally based on the material properties of the machined and ground specimen whether they are for endurance limit or the ultimate strength. The fatigue strength is function of material, component size, notch sensitivity, surface roughness etc. Hence the component needs to be tested. To account for the process variation number of components are tested for endurance. For the connecting rod under study it may be a costly affair to build the complete engine to study the reliability. The components like connecting rods are tested for fatigue by staircase method.

In staircase method, specimens are tested sequentially, with first one being tested at a load level equal to the estimated median fatigue limit, using preliminary information to define this value. If first specimen withstands the load level, second specimen is tested at higher load level. If the first specimen fails before reaching pre-decided number of load cycles, second specimen is tested a lower load level. Load levels thus jump up or down, depending on whether current test specimen fails or survives. The fixture should be made strong enough to sustain the higher fatigue loads. The fixture is not supposed to fail earlier than the sample connecting rods.

To facilitate the evaluation in both applications viz., power generation and industrial, by a single series of fatigue test, the two most severe cases are generally selected for the basis of test loading. The maximum tensile and compressive forces in the operating conditions are estimated. The safety margin factor of say 1.4 is applied at the start of the stair case method with an incremental step of 0.2. Mean safety factor and standard deviation are calculated statistically. Figure 13.3 shows Safety Coefficient for connecting rods by staircase method (Wani et al. 2005).

During testing on the rig, the specimen under test must be produced with due care to represent the final components. The assembly needs to be done carefully so that no additional loading is induced because of the misalignment.

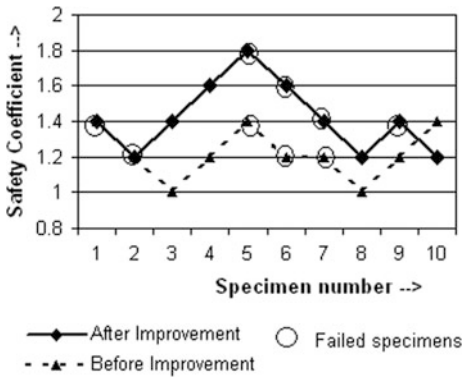

Fig. 13.3 Safety Coefficient for connecting rods by staircase method (Wani et al. 2005)

13.7 Improvement in Fatigue Strength

Fatigue strength of the connecting rod can be improved by shot peening process. In shot-peening, the steel balls are bombarded with help of nozzles on the rod. The shot-peening may be done only on un-machined part of the connecting rod.

Due to balls impacting on the rod a layer of compressive stress is created. The improvement in the fatigue strength is a function of intensity of shot peening and the depth of peening surface. The fatigue strength of the forged surface of the rod is lower than that of the machined smooth surface. Shot peening on forged surface help to improve the fatigue strength.

The impact of decarburization on fatigue life was investigated by Ilia and Chernenkoff (2001). They concluded that decarburized layer depths equal to or higher than 0.4 mm decrease the fatigue life.

13.8 Connecting Rods Produced by Fracture Splitting

The big end of a steel connecting rod is split by a method known as "Fracture splitting" method. It is separated by producing a fine crack from two notches using hydraulic force. For the split surfaces to be precise and to retain the shape and dimensions of the connecting rod during the process of splitting, the fracture should be brittle in nature. Normally forged steel connecting rod undergoes plastic deformation before actual fracture and hence is not suitable for this process. In case of carburised low carbon steel, the core of the fracture will not be brittle. Generally, C70 steel is used because of its crackability, higher strength and lower cost. It may be possible to further reduce the weight at the small and big ends using other facture crackable materials like micro-alloyed steels. Weight of the shank region cannot be easily reduced due to limitations of manufacturing constraints. To avoid the multiple fracture surfaces in-depth study is done from non-linear simulations (Kubota et al. 2004).

Some of the process steps in the conventional manufacturing sequence are eliminated like machining of the mating faces of the cap and rod, and drilling and reaming for dowels. About 25% reduction in production cost and 15% reduction in overall cost are achieved by this process. The distinct surface of the cracked surface restricts the relative movement of the rod and cap, providing firmness and stiffness to the joint. In addition, the stresses at critical locations at the split are reduced.

13.8.1 Process Sequence for Connecting Rod by Fracture Split

- Rough Grinding Rod
- Small End (S.E.) Drilling and Boring
- Bolt Seat milling
- Bolt Hole Drilling and Tapping
- Big End (B.E.) semi finish Boring
- Laser notching
- Fracturing
- Assembly of Rod and Cap.
- B.E. Facing and Chamfer
- B.E. Finish and S.E. Bush Bore
- Notch Milling
- B.E. Honing
- Deburring and Cleaning

It has been seen that laser notching exhibited best fracture splitting results, when compared with broached and wire cut notches. Research on development of lightweight connecting rods based on fatigue resistance analysis of micro alloyed steel was conducted by Kuratomi et al. (1990). The study found that the micro alloyed steel exhibits lower fatigue strength than the quenched and tempered steel for smooth specimens, but equivalent or higher fatigue strength for notched specimens.

High fatigue strength free machining micro alloyed steel was developed and used for connecting rods by Nakamura et al. (1993). The influence of alloy elements such as C, Mn, Cr, V, S, Pb, and Ca, and their impact on fatigue strength and machinability were discussed. A 0.33%C-1.05%Mn-0.5%Cr-0.12%V-0.55% S-0.20%Pb–Ca composition was found to be the best composition to improve fatigue strength.

For the cap splitting process, the connecting rods had 45° notches about 0.5 mm deep, machined on the sides of the bore and on the edges of the rod in the same plane as the bore notches.

13.8.2 Costing Comparison

Despite the substantially lower weight of the material used, however, the cost of the powder forged rough stock could be higher than that for the conventional hot drop-forged rough stock, because of additional operations of powder formation, pre-form formation, pre-sintering, and sintering (Afzal and Fatemi 2004). With recent introduction of new materials such as C-70 splittable steel, this key advantage of powder metal connecting rods no longer exists, as machining of matching

surfaces of splittable steel are no longer required. As mentioned in the literature review, fracture-split technology as applied to forged steel connecting rod cuts the total cost by 25%, compared to the conventional forged steel connecting rod. Dipak et al. (2010), Kubota et al. (2004), Ashley (1991).

The C-70 steel has higher strength than the powder metal material. Other alternative steels are also being developed with higher fatigue strength. Micro-alloyed 36 MnVS4 steel shows better fatigue strength than C-70 steel. For this new micro-alloyed steel, the component tests on materials showed 15–20% increase in fatigue strength (Pravardhan and Ali 2005).

For fracture split connecting rod it is important to have the parting at the expected plane, typically like the conventional parting line made by slitting process. One notch machined on the rod before fracture may not give this expected result. The crack does not propagate along a straight plane and it makes the section weak. The crack is shown in Fig. 13.4. Additional notches on the top and bottom surface are sometimes tried as shown in red, Fig. 13.5.

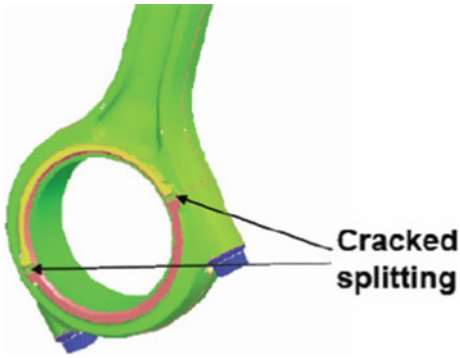

Fig. 13.4 Crack formation during fracture splitting of the connecting rod, by providing notches on the interior surface of the big end bore

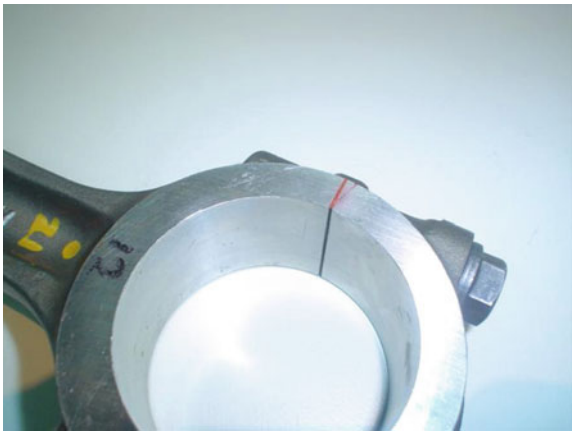

Fig. 13.5 Additional notches on the big end, on the top and bottom surface

13.9 Failure Modes

Figures 13.6, 13.7 and 13.8 show the modes of failure of the connecting rods.

Generally, connecting rod failure is due to fatigue and often it is seen at the junction of small end to I-section. The rod in Fig. 13.5 seems to have run for number of hours even after the breakage. The rods in Figs. 13.5 and 13.6 once again appear to be failing at the small end due to fatigue and high compressive load. The failure of connecting rod may be caused sometimes due to the fold defect during forging process. Hydraulic shock due to leakage of water in the cylinder chamber can sometimes create a very high pressure resulting into severe bending of a connecting rod.

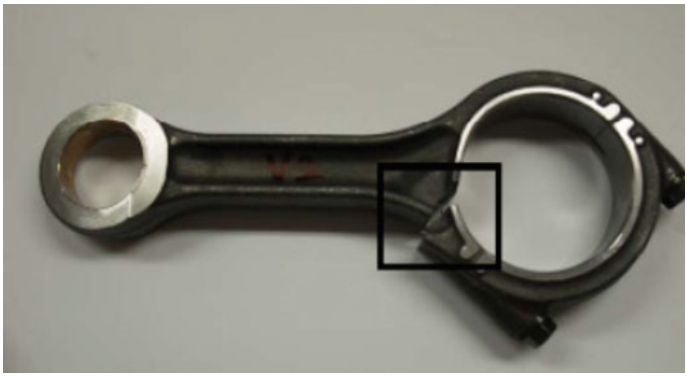

Fig. 13.6 A failure of a connecting rod at junction of small end

Fig. 13.7 A failure of a connecting rod at small end (Wani et al. 2005)

Fig. 13.8 A failure of a connecting rod at small end

Acknowledgements Authors acknowledge with thanks SAE, Society of Automotive Engineers for granting the permission to use Figs. 13.3 and 13.7 from reference (Wani et al. 2005) through Copyright Clearance Centre, www.copyright.com. They are thankful to "Sulzer Tech. Review and Sulzer Management Limited, Switzerland" for permitting to use the Figs. 13.13, 13.14, 13.15, 13.16 and 13.17 along with the equations in Annexure III from reference (Bremi 1971).

Appendix 1

Distribution of connecting rod mass at small end and big end (refer Figs. 13.9 and 13.10)

Let

$$L = \textit{centre distance between Small end and big end}$$
$$L_1 = \textit{distance of the Centre of gravity } (CG) \textit{ from the small end}$$
$$L_2 = \textit{distance of } CG \textit{ from big end}$$
$$L = L_1 + L_2$$

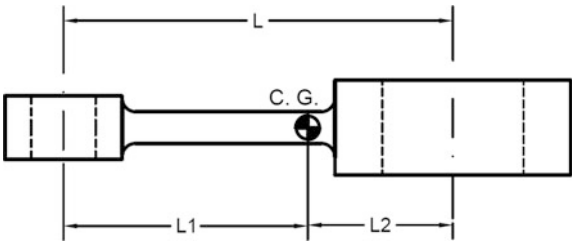

Fig. 13.9 Location of C.G. for the connecting rod

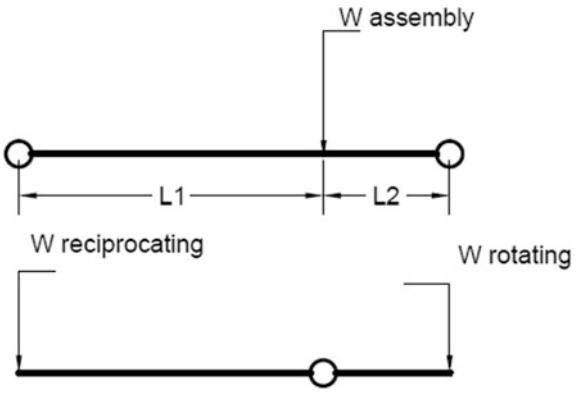

Fig. 13.10 Distribution of reciprocating and rotating masses for con rod

$$W_{assly} = \textit{weight of connecting rod assembly}$$
$$W_{recip} = \textit{reciprocating portion of the connecting rod assembly}$$
$$W_{rot} = \textit{rotating portion of the connecting rod assembly}$$
$$W_{assly} = W_{recip} + W_{rot}$$

Also, the moment of forces at CG is zero.

$$W_{recip} \times L_1 - W_{rot} \times L_2 = 0$$

Therefore,

$$W_{rot} = \left(\frac{L_1}{L_2}\right) W_{recip}$$
$$W_{assly} = W_{recip}\left(\frac{L_1 + L_2}{L_2}\right) \text{ Or } W_{recip} = W_{assly}\left(\frac{L_2}{L_1 + L_2}\right)$$

$$L = \textit{centre distance between the small end and the big end}$$
$$R = \textit{crank radius}$$
$$\theta = \textit{crank angle}$$
$$\varphi = \textit{obliquity angle}$$
$$x = \textit{displacement of piston assembly from the TDC at } \theta$$

From the Fig. 13.11,

$$L + R = x + L\cos\varphi + R\cos\theta$$
$$\therefore x = (L + R) - (L\cos\varphi + R\cos\theta)$$

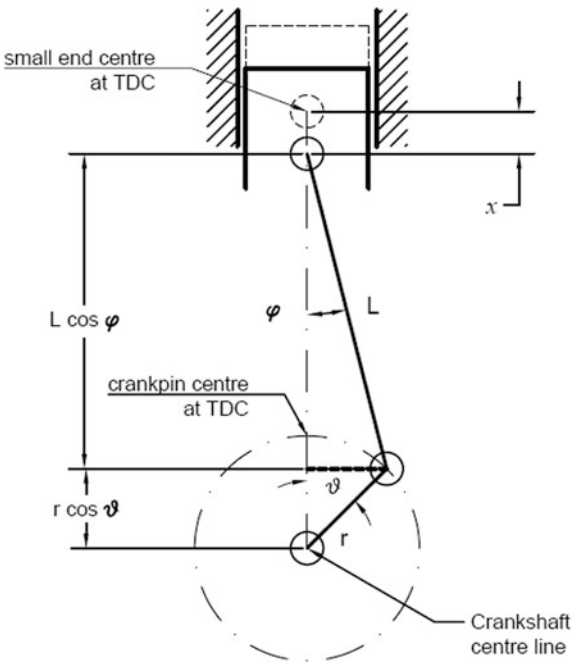

Fig. 13.11 Sketch of connecting rod at crank angle θ

But, $L \sin \varphi = R \sin \theta$

$$\frac{x}{R} = \left(1 + \frac{1}{\lambda}\right) - \cos\theta - \frac{1}{\lambda}\sqrt{1 - \lambda^2 sin^2\theta}$$

Where

$$\lambda = \frac{R}{L}$$

Fourier development of the equation gives

$$\frac{x}{R} = A_0 + A_1 \cos\theta - \frac{A_2}{4}\cos 2\theta + \frac{A_4}{16}\cos 4\theta - \frac{A_6}{36}\cos 6\theta + \cdots$$

Getting the values of A_0, A_1, A_2… in terms of λ and neglecting higher order terms of λ, λ being less than 1, we get,

i.e.

$$\frac{x}{R} = 1 + \frac{\lambda}{4} - \cos\theta - \frac{\lambda}{4}\cos 2\theta$$

$$velocity, v = \dot{x} = \omega R\left(\sin\theta + \frac{\lambda}{2}\cos 2\theta\right)$$

$$acceleration, a = \dot{v} = \ddot{x} = \frac{dv}{d\theta}\frac{d\theta}{dt} = \frac{dv}{d\theta}\omega$$

$$= R\omega^2\left(\cos\theta + \frac{\cos 2\theta}{n}\right)$$

Where

$$n = \frac{1}{\lambda}$$

$$\therefore Inertiaload = m_{recip} \times acceleration = m_{recip}R\omega^2\left(\cos\theta + \frac{\cos 2\theta}{n}\right)$$

Appendix 2

Inertia of I-section

The connecting rod small end and big end form a hinged joint in one plane where bend is tested. The other plane where twist is tested, the rod has more resistance to bending against the compressive load. In the latter case, the equivalent length is given below calculating the slenderness ratio.

$$l = \frac{l_{actual}}{2}$$

Hence to have the connecting rod equally strong about the both the axes, the critical buckling load, F_i should be such that

$$F = \frac{f_c A}{1 + \alpha\left(\frac{l}{R_{xx}}\right)^2} = \frac{f_c A}{1 + \alpha\left(\frac{l}{2R_{yy}}\right)^2}$$

i.e.

$$\left(\frac{1}{R_{xx}}\right)^2 = \left(\frac{1}{R_{yy}}\right)^2$$

or $I_{xx} = I_{yy}$ since $I = AR^2$ we get

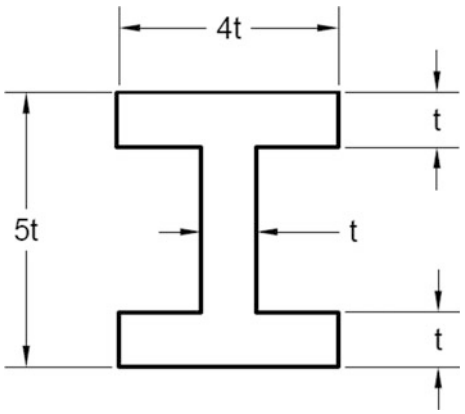

Fig. 13.12 Typical dimensions of I section

$$I_{xx} = 4I_{yy}$$

With the I-section defined by 4 *t*. 5 *t*. *t* as shown in the Fig. 13.12. This selection of cross section is taken as a starting guide line.

Appendix 3

Calculation of the connecting rod Big end (Bremi 1971)

Stresses at the big end is arrived at by the theory of curved beams. The big end is pulled by the inertia forces. Half connecting rod split by the plane passing through the centre line of the cylinder can be imagined as a hook. The shear and normal forces and the bending moment at the split. Since the split is in equilibrium the two halves of the connecting rod the respective forces on the faces are equal.

The reader is referred to the work done by P. Bremi (Bremi 1971). The formulae involved in brief are shown below. Refer Figs. 13.13, 13.14, 13.15 and 13.16 for simplified connecting rod model.

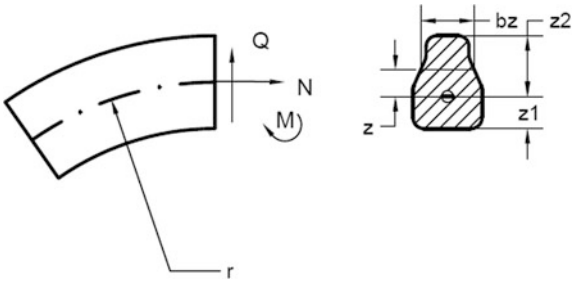

Fig. 13.13 Big end of connecting rod as a curved beam (Bremi 1971)

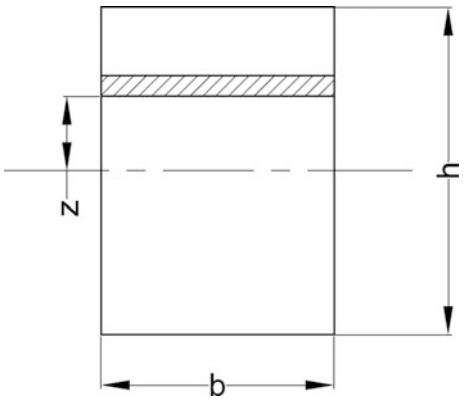

Fig. 13.14 Simplified rectangular cross section (Bremi 1971)

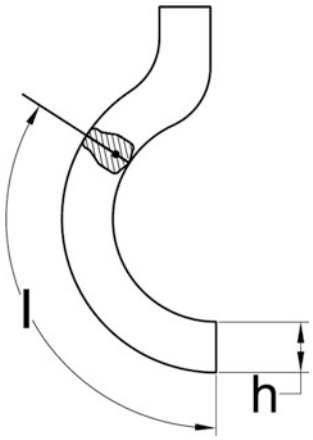

Fig. 13.15 Location of general cross section (Bremi 1971)

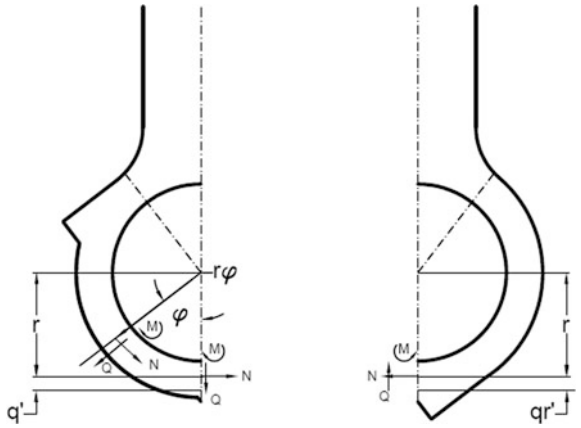

Fig. 13.16 Sketch showing various parameters of big end (Bremi 1971)

Bending stress,

$$\sigma(z) = \frac{N}{F} + \frac{M}{rF} + \frac{M}{r\lambda F}\frac{z}{r+z} \tag{13.1}$$

where

$$\lambda F = -\int_{z_1}^{z_2} \frac{z}{r+z} b(z)dz \tag{13.2}$$

$$I(z)(r+z)b(z) = -\frac{\Delta\lambda F}{\lambda F}Q + \int_{z_1}^{z} I(z')b(z)dz' \tag{13.3}$$

where

$$\Delta\lambda F = -\int_{z_1}^{z} \frac{z'}{r+z'} b(z')dz' \tag{13.4}$$

If

$$\Delta F = \int_{z_1}^{z} b(z')dz' \tag{13.5}$$

Then

$$I(z) = \frac{Q}{b(z)(r+z)}\left[\frac{\Delta F}{F} - \frac{\Delta\lambda F}{\lambda F}\right] \tag{13.6}$$

Deformation energy of the curved beam

$$\overline{U} = \frac{\sigma^2}{2E} \tag{13.7}$$

$$U = \int_{\phi_1}^{\phi_2}\int_{z_1}^{z_2} \frac{\sigma^2}{2E}(r+z)b(z)dzd\phi \tag{13.8}$$

Substituting from (13.1)

$$U = \int_{\phi_1}^{\phi_2} \frac{1}{2E}\left[\frac{N_r^2}{F} + 2\frac{NM}{F} + \frac{M^2}{rF}\left(1+\frac{1}{\lambda}\right)\right]d\phi \tag{13.9}$$

$$I(z) = \frac{Q}{6h^3}\left(\frac{h^2}{4} - z^2\right) \tag{13.10}$$

For comparison, a still simpler equation

$$J'(z) = \frac{Q}{bh} \tag{13.11}$$

$$\overline{U}_Q = \frac{J^2}{2G}, \tag{13.12}$$

where G = shear modulus

$$G = \frac{E}{2(1+\gamma)}, \tag{13.13}$$

where γ = Poisson ratio

Deformation energy of a beam piece of length, l

$$U_Q = \int_0^l \int_{-h/2}^{h/2} \frac{J^2}{2G} b\, dz\, dx \tag{13.14}$$

Substituting (10) and (11) in the above equation,

$$\textit{Deformation energy due to } Q, U_Q = \int_0^l \frac{3}{5}\frac{Q^2}{Gbh} dx \tag{13.15}$$

Or

$$U'_Q = \int_0^l \frac{1}{2}\frac{Q^2}{Gbh} dx \tag{13.16}$$

When the beam is loaded with moment M,

$$\textit{Deformation energy due to } M, U_M = \int_0^l \frac{6M^2}{Ebh^3} dx \tag{13.17}$$

If the beam is loaded at the end with a force P,

$$Q = P \tag{13.18}$$

and

$$M = Px \tag{13.19}$$

$$U = \frac{2P^2 l^3}{Ebh^3}\left[1 + \frac{3}{5}(1+v)\frac{h^2}{l^2}\right] \tag{13.20}$$

Or

$$U' = 2\frac{P^2 l^3}{Ebh^3}\left[1 + \frac{1}{2}(1+v)\frac{h^2}{l^2}\right] \tag{13.21}$$

In general case of a connecting rod,
If

$$v = \frac{1}{3}\ and\ l = 3h$$

Then,

$$U = \frac{2P^2 l^3}{Ebh^3}[1 + 0.09] \tag{13.22}$$

And

$$U' = 2\frac{P^2 l^3}{Ebh^3}[1 + 0.06] \tag{13.23}$$

The shear stress is not negligible since its contribution to the distortion energy is about 10% of that of the normal stress. Since *U*is within 1% of *U'* is only 1% Eq. 13.11 is used without loss of accuracy, instead of Eq. 13.10 while calculating the distortion energy.

For a bent beam,

$$J(z) = \frac{Q}{F} \tag{13.24}$$

$$UQ = \int_{\phi_1}^{\phi_2} \frac{1}{2G}\frac{Q^2}{F} r d\varphi \tag{13.25}$$

This energy can have the energy as Eq. 13.9 superimposed on it so that the following formula is valid for the deformation energy of the bent beam.

$$U = \int_{r_1}^{r_2} \frac{1}{2EF}\left[rN^2 + 2NM + \frac{1+\frac{1}{\lambda}}{r}m^2 + r\frac{E}{G}Q^2\right] d\phi \tag{13.26}$$

Displacement due to $N^l = n^l$
Displacement due to $Q^l = q^l$
Displacement due to $M^l = m^l$
Ref Fig. 13.16

We define

$$\alpha = \pi - \beta \tag{13.27}$$

And

$$K_\phi = \left\{0 for\, 0 \le \phi \le \frac{\pi}{2}, K for\, \frac{\pi}{2} \le \phi \le \alpha\right\} \tag{13.28}$$

for the split beam shown in figure.

In the split beam, there will be no load N, φ and C, moment created in the section of the connecting rod. The following relationships are obtained.

$$N_\phi = N\cos\phi + Q\sin\phi - K_\phi\cos\phi \tag{13.29}$$

$$Q_\phi = -N\sin\phi + Q\cos\phi + K_\phi\sin\phi \tag{13.30}$$

Moment of inertia of all forces at the centre of connecting rod,

$$M_\phi = N\left(r_0 - r_\phi\cos\phi\right) - Qr_\phi\sin\phi + K_\phi\sin\phi \tag{13.31}$$

Substituting in Eq. 13.26, the equations for deformation energy of half big end are as follows:

$$\begin{aligned} U = \frac{1}{2}\big[&a_{NN}N^2 + a_{NQ}NQ + a_{NM}NM + a_{NK}NK + a_{QN}QN + a_{QQ}Q^2 \\ &+ a_{QM}QM + a_{QK}QK + a_{MN}MN + a_{MQ}MQ + a_{MQ}MQ + a_{MM}M^2 + a_{MK}MK \\ &+ a_{KN}KN + a_{KQ}KQ + a_{kM}KM + a_{KK}K^2\big] \end{aligned} \tag{13.32}$$

$$\begin{aligned} a_{NN} = \int_0^\alpha \frac{r_\phi}{EF}\Bigg[&\cos^2\phi + 2\frac{r_\phi}{r}\left(\frac{r_0}{r_\phi} - \cos\phi\right) + \left(1 + \frac{1}{\lambda}\right)\frac{r_\phi^2}{r^2}\left(\frac{r}{r_\phi} - \cos\phi\right)^2 \\ &+ \frac{E}{G}\sin^2\phi\Bigg]d\phi \end{aligned} \tag{13.33}$$

$$a_{QQ} = \int_0^\alpha \frac{r_\phi}{EF}\left[\sin^2\phi - 2\frac{r_\phi}{r}\sin^2\phi + \left(1 + \frac{1}{\lambda}\right)\frac{r_\phi^2}{r^2}\sin^2\phi + \frac{E}{G}\cos^2\phi\right]d\phi \tag{13.34}$$

$$a_{MM} = \int_0^\alpha \frac{r_\phi}{EF}\left[\left(1 + \frac{1}{\lambda}\right)\frac{r_\phi^2}{r^2} - \frac{1}{r_\phi^2}\right]d\phi \tag{13.35}$$

$$a_{QM} = a_{MQ} = \int_0^{\alpha} \frac{r_\phi}{EF}\left[\frac{r_\phi}{r}\sin\phi\frac{1}{r_\phi} - \left(1+\frac{1}{\lambda}\right)\frac{r_\phi^2}{r^2}\sin\phi\frac{1}{r_\phi}\right]d\phi \tag{13.36}$$

$$a_{MN} = a_{NM} = \int_0^{\alpha} \frac{r_\phi}{EF}\left[\frac{r_\phi}{r}\cos\phi\frac{1}{r_\phi} + \left(1+\frac{1}{\lambda}\right)\frac{r_\phi^2}{r^2}\left(\frac{r}{r_\phi} - cos\phi\right)\frac{1}{r_\phi}\right]d\phi \tag{13.37}$$

$$\begin{aligned} a_{NQ} = a_{QN} = \int_0^{\alpha} \frac{r_\phi}{EF}\Bigg[&\cos\phi\sin\phi - \frac{r_\phi}{r}\cos\phi\sin\phi + \frac{r_\phi}{r}\sin\phi\left(\frac{r}{r_\phi} - \cos\phi\right) \\ &- \left(1+\frac{1}{\lambda}\right)\frac{r_\phi^2}{r^2}\left(\frac{r}{r_\phi} - cos\phi\right)\sin\phi - \frac{E}{G}\sin\phi\cos\phi\Bigg]d\phi \end{aligned} \tag{13.38}$$

$$\begin{aligned} a_{NK} = a_{KN} = \int_0^{\alpha} \frac{r_\phi}{EF}\frac{K_\phi}{K}\Bigg[&-\cos^2\phi + \frac{r_\phi}{r}\cos^2\phi - \frac{r_\phi}{r}\cos\phi\left(\frac{r}{r_\phi} - \cos\phi\right) \\ &-\left(1+\frac{1}{\lambda}\right)\frac{r_\phi^2}{r^2}\left(\frac{r}{r_\phi} - cos\phi\right)\cos\phi - \frac{E}{G}\sin^2\phi\Bigg]d\phi \end{aligned} \tag{13.39}$$

$$\begin{aligned} a_{QK} = a_{KQ} = \int_0^{\alpha} \frac{r_\phi}{EF}\frac{K_\phi}{K}\Big[&-\sin\phi\cos\phi + \frac{r_\phi}{r}\sin\phi\cos\phi \\ &-\left(1+\frac{1}{\lambda}\right)\frac{r_\phi^2}{r^2}\sin\phi\cos\phi - \frac{E}{G}\sin\phi\cos\phi\Bigg]d\phi \end{aligned} \tag{13.40}$$

$$a_{MK} = a_{KM} = \int_0^{\alpha} \frac{r_\phi}{EF}\frac{K_\phi}{K}\left[-\frac{r_\phi}{r}\cos\phi\frac{1}{r_\phi} + \left(1+\frac{1}{\lambda}\right)\frac{r_\phi^2}{r^2}\cos\phi\frac{1}{r_\phi}\right]d\phi \tag{13.41}$$

$$a_{KK} = \int_0^{\alpha} \frac{r_\phi}{EF}\frac{K_\phi^2}{K^2}\left[\cos^2\phi - 2\frac{r_\phi}{r}\cos^2\phi + \left(1+\frac{1}{\lambda}\right)\frac{r_\phi^2}{r^2}\cos^2\phi + \frac{E}{G}\sin^2\phi\right]d\phi \tag{13.42}$$

Stresses on the big end

$$n = \frac{\partial U}{\partial N} = a_{NN}N + a_{NQ}Q + a_{NM}M + a_{NK}K \tag{13.43}$$

$$q = \frac{\partial U}{\partial Q} = a_{QN}N + a_{QQ}Q + a_{QM}M + a_{QK}K \tag{13.44}$$

$$m = \frac{\partial U}{\partial M} = a_{MN}N + a_{MQ}Q + a_{MM}M + a_{MK}K \tag{13.45}$$

To these we add the following quantity

$$k = \frac{\partial U}{\partial K} = a_{KN}N + a_{KQ}Q + a_{KM}M + a_{KK}K \tag{13.46}$$

For the above calculations, the connecting rod is assumed to be split. In actual case, it is not. Now,

$$N^l = N^r \tag{13.47}$$

$$Q^l + Q^r = P \tag{13.48}$$

$$M^l = M^r \tag{13.49}$$

$$n^l = -n^r \tag{13.50}$$

$$q^l = q^r \tag{13.51}$$

$$m^l = -m^r \tag{13.52}$$

A set of linear equations for the six unknowns N^l, Q^l, m^l, N^r, Q^r and M^r is obtained using Eqs. 43–45 for each half of the big end. This system can be easily converted back to the system

$$(a^l_{NN} + a^r_{NN})N^l + \left(a^l_{NQ} - a^r_{NQ}\right)Q^l + (a^l_{NM} + a^r_{NM})M^l = -a^r_{NQ}P - a^l_{NK}K^l - a^r_{NK}K^r \tag{13.53}$$

$$\left(a^l_{QN} - a^r_{QN}\right)N^l + \left(a^l_{QQ} + a^r_{NQ}\right)Q^l + \left(a^l_{QM} - a^r_{NM}\right)M^l = a^r_{QQ}P - a^l_{QK}K^l + a^r_{QK}K^r \tag{13.54}$$

$$\begin{aligned}(a^l_{MN} + a^r_{MN})N^l + \left(a^l_{MQ} - a^r_{MQ}\right)Q^l + (a^l_{MM} + a^r_{MM})M^l \\ = -a^r_{MQ}P - a^l_{MK}K^l - a^r_{MK}K^r\end{aligned} \tag{13.55}$$

This selection of cross section is taken as a starting guide line. The calculations are iterated for the modified configuration, depending on the magnitude of the stresses. A typical stress distribution is shown in Fig. 13.17.

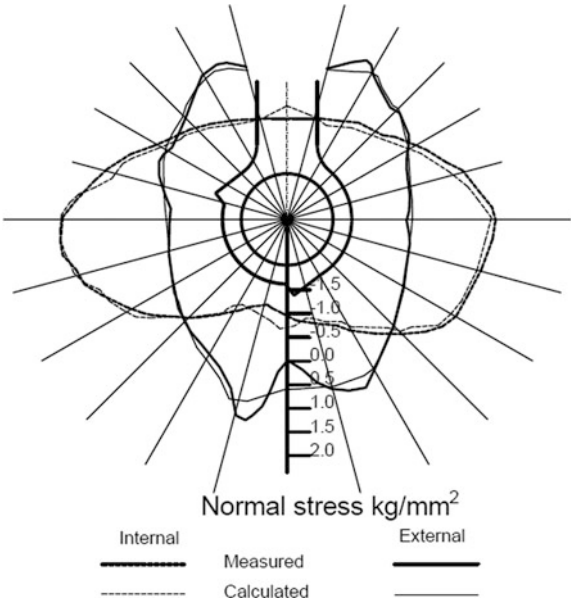

Fig. 13.17 Stresses in big end of the connecting rod (Bremi 1971)

Appendix 4

Connecting rod Big end bolt sample calculation

The calculations are performed for a connecting rod having two bolts. The side force Q is not considered as the rod assumed with horizontal split.

Bolt sizeM12 × 1.5
Bolt Quality10.9
$m_{recip.}$ 1.720 kg.
m_{rod} without cap1.305 kg.

$$r = crank\ radius = 0.054\,\text{m}$$

$$\varpi = \frac{2\pi n}{60} where\ n = 3150\ rpm\ 330\,\text{rad/sec.}$$

$$L = con.\ rod\ centre\ distance\ 0.187\,\text{m}$$

$$Fmax = (m\ recip + m\ rod)r\varpi 2\left(1 + \frac{r}{L}\right) 22925\,\text{N}$$

Bolt torque10 kgm with oil (80% yield)
Preload as per VDI 2230 (VDI 2230) is estimated as 54004 N per bolt
Total preload108008 N
The force $F_{interference}$ due to bearing overstand-
Assuming 25 kg/mm^2 stress on bearing,

$$\begin{aligned}
\text{The dimensions of bearings:} \quad & 2\,\text{mm thick} \times 23\,\text{mm length} \\
Area\ on\ one\ side &= 46\,\text{mm}^2 \\
Force\ on\ each\ side\ 25 \times 46 &= 1150\,\text{kg} \\
Force\ on\ both\ sides &= 2300\,\text{kg} \\
Force\ on\ each\ bolt &= 1150\,\text{kg} \\
\therefore Finterference &= 11280\,\text{N} \\
\therefore Total\ load\ on\ bolt & \\
&= Fmax + Finterference \\
&= 22925 + 11280\,\text{N} \\
&= 34205\,\text{N} \\
\therefore Cover\ factor &= \frac{108008}{34205} \\
&= 3.16 > 2 \\
Hence\ safe &
\end{aligned}$$

Connecting rod Big end bolt detailed calculation as per VDI 2230

The connecting rod big end joint as shown in Fig. 13.18 is example of eccentrically clamped eccentrically loaded joint. The analysis is to be done for 12.9 grade M9 × 1 bolt and grade-12 nut.

The bolts are tightened with a high precision tightening spindle. C45 was selected as the material for the clamped parts. For the rated engine speed (n = 4000 rpm), we have the following initial parameters.

Axial force at the interface

$$Fa = 3.7 \times 10^3\,\text{N}$$

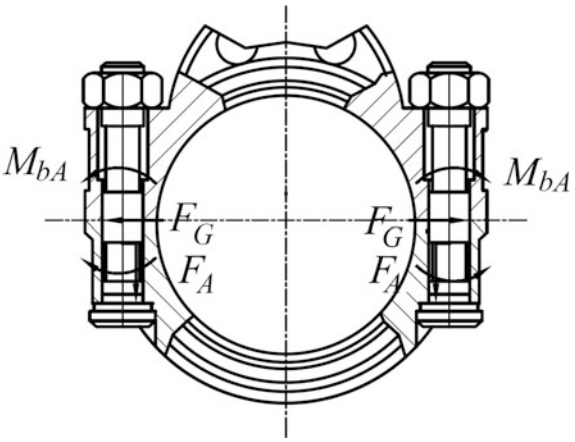

Fig. 13.18 Forces acting on the interface of a connecting rod bearing cap bolted joint

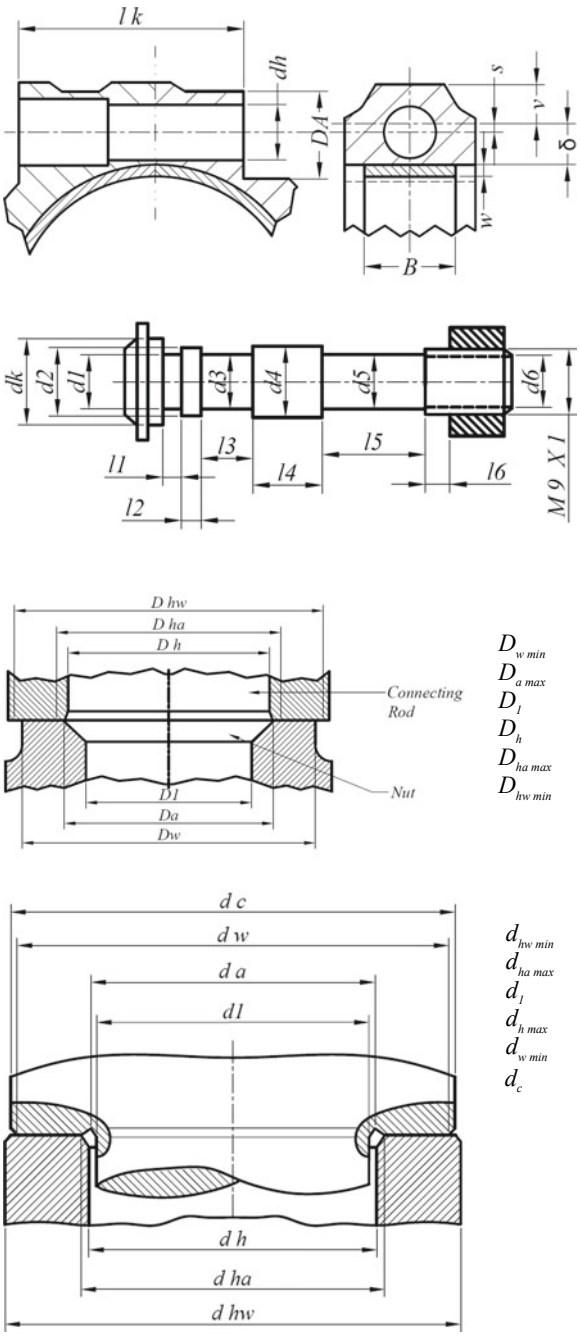

$D_{w\,min}$	13.8
$D_{a\,max}$	9.9
D_{l}	7.9
D_{h}	9.43
$D_{ha\,max}$	10
$D_{hw\,min}$	14

$d_{hw\,min}$	14
$d_{ha\,max}$	9.65
d_{l}	9.25
$d_{h\,max}$	9.0
$d_{w\,min}$	13.2
d_{c}	13.4

Fig. 13.19 Dimensions(mm) of the clamping and clamped parts of the connecting rod bearing cap bolted joint and the nut and head bearing surfaces

Bending moment at the interface

$$M_{bA} = 30\,\text{Nm}$$

Transverse force at the interface

$$F_Q = 420\,\text{N}$$

From the bending moment M_{bA} and the axial load F_A, the lever arm of the eccentric load application is determined as

$$a = \frac{M_{bA}}{F_A} = 8.1\,\text{mm}$$

Assuming for simplicity that the bending moment is constant over the clamping length l_K

Calculation procedure

The calculations are made following the calculations steps R1 to R10 given in Sect. 4.1 VDI 2230.

R1Rough determination of the bolt diameter d and the clamping length ratio l_K/d.

The bolt diameter is given as 9 mm from the design shown in Fig. 13.19. The clamping length ration is

$$\frac{l_K}{d} = \frac{41.5}{9} = 4.6$$

Rough determination of the surface pressure under the bolt head:

$$p = \frac{\frac{F_{IA}}{0.9}}{A_P} \leq P_G$$

Measurement of screw in mm

Place	l_1	d_1
	2.5	8.7
	3.0	9.2
	6.5	9.0
	10.0	9.2
	15.8	8.35
	3.7	7.68

Other Measurements

Thread		Clamped parts		Nut bearing		Head bearing	
d_2	8.27	D_A	15.5	$D_{w,\ min}$	13.8	$d_{hw,\ min}$	14
d_3	7.66	d_b	9.25	$D_{b,\ max}$	9.9	$d_{ho,\ min}$	9.65
d	9	l_g	41.5	D_1	7.9	d_h	9.25
P	7	g	0.3	d_h	9.43	d_f	8.7
A_{d3}	46 mm^2	a	8.1	$D_{h0,\ max}$	10	$d_{b,\ max}$	9
		u	5.3	$D_{h0,\ min}$	14	$d_{w,\ min}$	13.2
		v	6.8			d_p	13.4
		w	1.4				
		n	17.6				

$F_M = 42.6 \times 10^3\,\mathrm{N}\, for\, \mu_G = 0.12$ from Table 3 of VDI 2230.
With

$$A_{P\,head,min} = \frac{\pi}{4}\left(d_{W,min}^2 - d_{h\,a,max}^2\right) = 64\,\mathrm{mm}^2$$

and

$$A_{Pnut,min} = \frac{\pi}{4}\left(D_{w,min}^2 - D_{ha,max}^2\right) = 71\,\mathrm{mm}^2$$

follows

$$P_{max} = \frac{F_M}{0.9\,A_{Phead,min}} = 740\,\frac{\mathrm{N}}{\mathrm{mm}^2} > P_G$$

where P_G = 700 N/mm^2 from Table 39 of VDI2230. Further examination in R10.

R2 Determination of the tightening factor α_A

The bolt is tightened using a high precision tightening spindle, which has been adjusted by measuring the elongation of the bolt (after pre-calibrating the bolt as the force measuring element).

The tightening factor α_A = 1.6 according to Table 8of VDI 2230 (for large angles of rotation, fine threads and resilient joints).

R3 Determination of the required minimum clamp load, $F_{K\,erf}$

1. The requirement for friction grip at the interface (μ_{Tr} = 0.12) is: $F_{K\,erf1} = \frac{F_0}{\mu_{Tr}} = 3.5 \times 10^3\,\mathrm{N}$
2. To avoid one-sided opening at the rated speed of the engine, $F_{K\ erf2}$ is calculated (from Eq. 3.52 of VDI 2230) using the dimensions given in Fig. 13.19.

$$F_{K\,erf_2} = \frac{(a-s)u}{\frac{I_{BT}}{A_D} + su} F_A = 8.1 \times 10^3\,\text{N}$$

Where

$$A_D = 121\,\text{mm}^2$$
$$I_{BT} = 2474\,\text{mm}^4$$

R4 Determination of the load factor, Φ_{en}

The transmission of bending moments and normal forces at the interface leads to a bolted joint with eccentric load application. Moreover, the load is not introduced under the bolt head and the nut but inside the clamped parts. Since the greater part of the connecting rod joint surrounding the bolt can be considered to be a clamping sleeve, n = 1/3 is estimated in this case.

With

$$A_{ers} = 122\,\text{mm}^2$$

Using Eq. (3.34 of VDI 2230)

$$\Phi_{en} = n\frac{\delta_P\left(1 + \frac{a_S A_{ers}}{I_{B\,ers}}\right)}{\delta_S + \delta_P\left(1 + \frac{s^2 A_{ers}}{I_{B\,ers}}\right)}$$

The resilience of the bolt is calculated using Eq. 3.8 of VDI 2230

$$\delta_S = \delta_K + \delta_1 + \delta_2 + \cdots + \delta_{GM}$$

Its components are found as follows

1. Thread elasticity in the nut:

$$\delta_G = \frac{0.5d}{E_S A_3} = 0.477 \times 10^{-6}\,\text{mm/N}$$

Where

$$E_S = 205 \times 10^3\,\text{N/mm}^2$$

2. Elasticity due to the displacement of the nut:

$$\delta_M = \frac{l_M}{E_S A_N} = 0.276 \times 10^{-6}\,\text{mm/N}$$

Where

$$l_M = 0.4\,d$$

3. Elasticity of the free and loaded part of the thread:

$$\delta_6 = \frac{l_6}{E_S A_3} = 0.392 \times 10^{-6}\,\text{mm/N}$$

4. Elasticity of the shank:

$$\delta_{1\cdots5} = \sum_{i=1\cdots5} \frac{l_i}{E_S A_N} = 3.064 \times 10^{-6}\,\text{mm/N}$$

5. Elasticity of the head:

$$\delta_K = \frac{0.4\,d}{E_S A_N} = 0.276 \times 10^{-6}\,\text{mm/N}$$

We thus have

$$\delta_S = \delta_G + \delta_M + \delta_6 + \delta_{1\cdots5} + \delta_K = 4.49 \times 10^{-6}\,\text{mm/N}$$

Resilience of the clamped parts δ_P:

For the determination of the resilience of the clamped parts, the small eccentricity of the bolt (s = 0.3) is not allowed for. Thus, δ_P will be determined instead of δ_P^*. The assembly preload which causes embedding acts concentrically. For a cross-section study of the clamped parts of a substitution body Fig. 13.5 of VDI 2230 should be referred. Since the joint has a clearance hole, with dimensions D_A and d_h, and because

$$d_w \le D_A \le d_w + l_K$$

We find with Eq. (3.17 of VDI 2230)

$$A_{ers} = 122\,\text{mm}^2$$

Where

$$D_A = 15.5\,\text{mm}; d_w = 13.2\,\text{mm}; l_K = 41.5\,\text{mm}; d_h = 9.25\,\text{mm}$$

With

$$E_P = 205 \times 10^3\ \text{N/mm}^2$$

We find

$$\delta_P = \frac{l_K}{E_P A_{ers}} = 1.66 \times 10^{-6}\ \text{mm/N}$$

Thus, with $I_{B\,ers}$ = 2833 mm^4 because D_{ers} = 15.5 mm determined from A_{ers} and d_h = 9.25 mm we obtain from Eq. (3.43) of VDI 2230

$$\Phi_{en} = 0.118$$

R5Determination of the loss of preload due to F_Z embedding

From Fig. 50 of VDI 2230 we find the amount of embedding f_Z = 6.1 $\times$ 10^{-3} mm (rounded), for l_K/d = 4.6. Thus, the loss of preload due to embedding,

$$F_Z = f_Z \frac{1}{\delta_P + \delta_S} = 0.976 \times 10^3\ \text{N}$$

R6 Determination of the required bolt size

The maximum assembly preload is calculated from:

$$F_{M\,\max} = \alpha_A \left[F_{K\,erf} + (1 - \Phi_{en})F_A + F_Z\right]$$

However, for the case of a bearing cap bolted joint, $F_{M\,min}$ must be further increased by the amount F_L required for the elastic and plastic deformation which occurs in the shell bearing because of over sizing.

To compensate for over-sizing of the shell bearings, an axial load F_L of 6.2 $\times$ 10^3 N per bolt is required.

Thus, in this case we have

$$F_{M\,\max} = \alpha_A \left[F_{K\,erf} + (1 - \Phi_{en})F_A + F_Z + F_L\right]$$

With

$$F_{K\,erf} = F_{K\,\text{erf}\,2}, since\ F_{K\,\text{erf}\,2} > F_{K\,\text{erf}\,1}$$
$$F_{M\,max} = 29.7 \times 10^3\ \text{N}$$

Assuming a coefficient of friction μ_G = 0.12 (Table 5 of VDI 2230), we obtain from Eq. (3.26 of VDI 2230) an assembly preload of

$$F_M = \sigma_M A_0 = 41.6 \times 10^3 \mathrm{N}$$

for the bolt M9 × 1 of strength grade 12.9. Therefore, $A_0 = A_s = 49.8\ \mathrm{mm}^2$ and

$$\begin{aligned}\sigma_M &= \frac{\nu R_{p\,0.2\,min}}{\sqrt{1+3\left[\frac{2d_2}{d_0}\left(\frac{P}{\pi d_2}+1.155\mu_G\right)\right]^2}} \\ &= 835\,\frac{\mathrm{N}}{\mathrm{mm}^2} \\ d_0 &= d_s = 7.963\,\mathrm{mm} \\ R_{p\,0.2} &= 1100\,\frac{\mathrm{N}}{\mathrm{mm}^2}\end{aligned}$$

And with $\nu = 0.9$, follows

$$F_M > F_{M\,max}$$

The dimensions of the bolt are correct.

With $\mu_K = 0.12$, we have a tightening torque of

$$\begin{aligned}M_A &= F_M\left(0.16P + \mu_G \times 0.58 d_2 + \frac{D_{k\,m}}{2}\mu_K\right) \\ &= 60.3\,\mathrm{Nm}\end{aligned}$$

where

$$\begin{aligned}\frac{D_{k\,m}}{2} &= \frac{D_{w\,min} + D_{ha\,max}}{4} = 5.95 \\ \mu_G &= 0.12\end{aligned}$$

R7 The check for l_K/d and Φ can be omitted since these values are already determined exactly.

R8 The check that the maximum permissible bolt force is not exceeded

$$\begin{aligned}&\Phi_{en} F_A \leq 0.1\, R_{p0.2\,\mathrm{min}} A_0 \\ &440\,N < 5480\,N\end{aligned}$$

R9 Determination of the alternating stress endurance of the bolt.

Because of the eccentric clamping and loading, the bolt is subject to tensile stresses and to bending stresses.

From Eq. (3.74 b of VDI 2230),

$$\sigma_{SA\,b} = \left[1 + \left(\frac{1}{\Phi_{en}} - \frac{s}{a}\right)\frac{l_K}{l_{ers}}\frac{E_s}{E_P}\frac{a\,\pi d_3^3}{8\overline{I}_{B\,ers}}\right]\frac{\Phi_{en}F_A}{A_{d3}}$$

It follows from

$$\Phi_{en} = 0.118, \frac{l_K}{l_{ers}} = 1, F_A = 3.7 \times 10^3 N, \frac{E_s}{E_p} = 1, \overline{I}_{B\,ers} = I_{B\,ers} - \frac{\pi d_h^4}{64}$$
$$= 2474\,\text{mm}^4$$

That on the side in tension

$$\sigma_{SA\,b} = (1 + 4.88) \times 9.49\frac{\text{N}}{\text{mm}^2}$$
$$= 9.5\frac{\text{N}}{\text{mm}^2} + 46.5\frac{\text{N}}{\text{mm}^2}$$
$$= 56\frac{\text{N}}{\text{mm}^2}$$

With strain gauges attached to the bolt shank in the vicinity of the interface, a tensile stress variation of 52 N/mm^2 and a compressive stress variation of –32 N/mm^2 relative to the pre-load were measured, after applying an axial force of F_A to a joint with minimum bolt pre-load $F_{V\,erf} = F_{K\,erf\,2} + F_L$. From this we obtain a tensile stress component of 10 N/mm^2 (9.5 N/mm^2 was calculated) and a bending stress component of 42 N/mm^2 (46.5 N/mm^2 was calculated). Figure 13.20 gives a comparison between the calculated and measured stress distribution in the interface plane of the bolt.

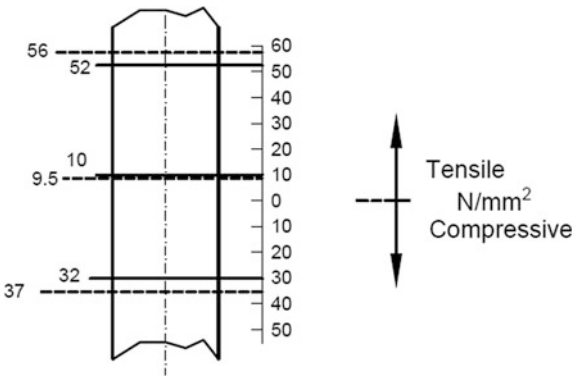

Fig. 13.20 Stress distribution in the interface plane of the bolt

On the tensile side, the bolt alternating stress is

$$\sigma_B = \frac{\sigma_{SA\,b}}{2} = \pm 28\,N/\mathrm{mm}^2$$

Figure 48 of VDI 2230 gives

$$\sigma_A = \pm 54\,N/\mathrm{mm}^2$$

Thus, we have $\sigma_B < \sigma_A$

R10 Checking calculation of the surface pressure under the head bearing

The nut bearing is not examined.

$$A_{P\,nut\,min} > A_{P\,head\,min},$$

See R1

$$p = \frac{F_M + \Phi_{en} F_A}{A_{P\,head\,\mathrm{min}}} = 660\,\frac{\mathrm{N}}{\mathrm{mm}^2}$$

$$p < p_G = 700\,\mathrm{N/mm}^2$$

p_G *value* is taken from Table 9 of VDI 2230.

The checking calculation shows that the function of the bolted joint, under strength stipulations is fulfilled.

Symbols and notations (VDI 2230)

A	Cross sectional area
A_D	Interface area minus the area of the hole for the bolt
A_{ers}	Equivalent cross section area of a hollow cylinder with the same elastic resilience of the clamped parts
A_P	bearing area of the bolt head or nut
D_A	Outside diameter of the clamped sleeve- for the interface surfaces of a varying circular form (d_A = the diameter of the inner circle)
D_a	Inner diameter of bearing surface of the nut
D_{ha}	Inner diameter of the bearing area of the clamped parts under the nut (at the start of the fillet of the clamped parts)
D_{hW}	Outside diameter of the bearing area of the clamped parts under the nut (at the thread or at the start of the fillet of the outside diameter)
D_W	Outside diameter of bearing area of the nut (at the start of the fillet of the outside of the nut)
D_f	minor diameter of the thread in the nut
E_P	Young's modulus of the parts clamped
E_s	Young's modulus of the bolt
F_A	Axial force calculated along the bolt axis or the components for a given working load, F_B

(continued)

(continued)

A	Cross sectional area
F_B	Working load in a joint in any direction
$F_{K\ erf}$	required clamping load for sealing functions, friction grip and prevention of one-sided opening at the interface
F_M	Initial clamping load (assembly preload); The values in tables of VDI 2230 are calculated with a 90% of the elastic limit using σ_{red}
$F_{M\ max}$	Initial clamping load for which the bolt is designed considering lack of precision in the tightening technique the expected bedding in during operation, the minimum required clamping load
$F_{M\ min}$	Minimum initial clamping load established at $F_{M\ max}$ because of lack of precision in the tightening technique
F_Q	Transverse force normal to bolt axis
F_V	Preload
$F_{V\ erf}$	Minimum preload required to ensure sealing functions, friction grip and one sided opening at the interface by loss of the force at the interface
F_Z	Loss of preload due to bedding in during operation
$I_{B\ ers}$	Equivalent area moment of inertia
$\overline{I}_{B\ ers}$	I_{Bers} minus area moment of inertia for the bolt hole
I_{BT}	Area moment of inertia for the interface
M_b	Bending moment at the bolting point due to the axial loads, F_A and F_S applied eccentrically
P	thread pitch
$R_{p\ 0.2}$	0.2% proof stress as per DIN ISO 898 Part 1
a	Distance at which the load acts from the axis of the surface A_B
d	Bolt diameter = outside diameter of the thread (nominal diameter)
d_a	Inner diameter of the face of the bolt head (at the inlet of the transition radius of the shank)
d_c	Core diameter of the face of the bolt head
d_h	Bore diameter of the clamped parts; inner diameter of the equivalent cylinder
d_{ha}	Inner diameter of the bearing surface of the bolt head (from the start of the fillet the bore)
d_{hW}	Outer diameter of the bearing surface of the clamped parts with the bolt head (from the start of the fillet of the outer diameter of the clamped parts)
d_W	Outside diameter of the plane head bearing surface (at the inlet of the transition radius of the head)
d_0	Diameter at the smallest cross section of the bolt shank
d_2	Pitch diameter of the bolt thread
d_3	Minor diameter of bolt thread
F_2	Plastic deformation by bedding in

(continued)

(continued)

A	Cross sectional area
l	Length, in general
li	Length of the bolt
l_t	Clamping length
n, $\bar{n}$	A factor given by the ratio of the thickness of sections of clamped parts unloaded by the axial load, F_A to the clamping length l_K
p	Surface pressure
p_G	maximum permissible pressure under a bolt head
s	Distance between the bolt and the axis of the surface A_B
u	Distance between the edge of clamped part (prism) from the axis of the surface A_B (in the direction opposite to A-A)
v	Distance between the edge in clamped part (prism) from the axis of the surface A_s (in the direction opposite to A-A)
α_A	Tightening factor, F_{Mmax}/F_{Mmin}
δ	Elastic resilience
δ_G	Resilience of engaged thread
δ_i	Resilience of any part, i
δ_K	Resilience of bolt head
δ_p	Resilience of the clamped parts for the concentric bolting and concentric loading
δ_{p*}	Resilience of the clamped parts for eccentric loading
δ_{p**}	Resilience of the clamped parts for eccentric bolting and eccentric loading
δ_s	Resilience of the bolt
μ_G	Coefficient of friction in the thread
μ_K	Coefficient of friction for bolt head
γ	A fraction of the yield load to which the bolt is tightened
σ_A	Stress amplitude at the endurance limit
σ_a	Alternating stress acting on the bolt
σ_M	Tensile stress due to F_M
σ_{red}	Equivalent stress, (relative stress)
$\sigma_{SA\,b}$	tensile stress (due to bending) in bolt thread caused by the axial load F_{SA} and the bending moment M_b due to eccentric application of load
$\sigma_{SA\,d}$	Same as σ_{SAb}, but compression stress due to bending
ϕ	Load factor, F_{SA}/F_A
ϕ_e	Load factor for eccentric application of axial load F_A
ϕ_{en}	Load factor, ϕ_e for introduction of load through the clamped parts
ϕ_n	Load factor for introduction of axial load F_A concentrically at a distance = $n\ l_K$

References

Afzal A, Fatemi A (2004) A comparative study of fatigue behaviour and life predictions of forged steel and PM connecting rods. No. 2004-01-1529. SAE Technical Paper

Ashley Steven (1991) Connecting rods that crack by design. Publication, Mechanical Engineering-CIME

Bremi P (1971) Calculation of the stresses and most important deformations on a connecting rod big end with the help of a computer. Sulzer Tech Rev, Switzerland 1:59–64

Dipak S, Khan AM, Jaipuria A (2010) Dynamic load analysis and optimization of a fracture-split connecting rod

Kubota T, Iwasaki S, Isobe T, Koike T (2004) Development of fracture splitting method for case hardened connecting rods. No. 2004-32-0064. SAE Technical Paper

Pravardhan SS (2004) Dynamic load analysis and optimization of connecting rod. PhD diss., The University of Toledo

Pravardhan SS, Ali F (2005) Connecting rod optimization for weight and cost reduction. No. 2005-01-0987. SAE Technical Paper

VDI 2230: Systematic calculation of heavy duty bolted joints: joints with one cylindrical bolt

Wani PR, Dani AD, Reddy PV (2005) Study of connecting rod for high BMEP engines. No. 2005–26-003. SAE Technical Paper

Ilia E, Chernenkoff RA (2001) Impact of decarburization on the fatigue life of powder metal forged connecting rods. No. 2001-01-0403. SAE Technical Paper

Kuratomi H, Uchino M, Kurebayashi Y, Namiki K, Sugiura S (1990) Development of lightweight connecting rod based on fatigue resistance analysis of microalloyed steel. SAE transactions 487–491

Nakamura S, Mizuno K, Matsubara T, Sato Y (1993) Development of high fatigue strength free machining microalloyed steel for connecting rods. SAE Transactions 858–865

Fatemi A, Zoroufi M, Shenoy P, Afzal A (2005) Comparative durability study of competing manufacturing process technologies. Mechanical, industrial and manufacturing engineering department, The university of toledo, toledo, ohio